Identifying Topological Phase Transitions in Experiments Using Manifold Learning

Eran Lustig,* Or Yair,* Ronen Talmon, and Mordechai Segev
Technion–Israel Institute of Technology, Haifa 32000, Israel

(Received 17 October 2019; accepted 7 July 2020; published 14 September 2020)

We demonstrate the identification of topological phase transitions from experimental data using diffusion maps: a nonlocal unsupervised machine learning method. We analyze experimental data from an optical system undergoing a topological phase transition and demonstrate the ability of this approach to identify topological phase transitions even when the data originates from a small part of the system, and does not even include edge states.

DOI: 10.1103/PhysRevLett.125.127401

Topological phases are currently at the heart of modern research due to their fundamental nature and potential applications. These phases are characterized by unique properties such as robust unidirectional edge states, exhibiting transport immune to scattering, and quantized conductance [1–3]. These distinct features were observed in many experiments and on different platforms [4–13]. However, numerous topological phases were predicted but thus far never observed in any experiment [14,15], and new topological phases are still being proposed theoretically [15] with the hope to be observed in the future. Experimentally, topological phases are typically identified by studying the features of the edge transport in the medium, through measuring properties such as conductance or photoemissivity (in solid state), or by imaging the transport of light waves, acoustic waves, etc. This creates major challenges because in many cases the system does not have a clear edge (e.g., cold atoms in magneto-optic traps), or because only bulk states are accessible in experiments. The challenge in observing topological phase transitions stems from their nonlocal nature, that is: the nontrivial topology is a property of the entire system, and not of a local part of it. Consequently, topological phase transitions can often be revealed only by specific excitations that require both a high degree of control over the system and a firm understanding of it [8,11].

Furthermore, modern experimental systems can produce large amounts of data with many degrees of freedom that are impossible to exploit without automation. These and other challenges exemplify the need for machine learning algorithms to identify and characterize topological phase transitions based on partial (incomplete) experimental data. In principle, neural networks can be trained on known phase transitions to detect an unknown phase transition in the Hamiltonian [16] or the entanglement spectrum [17], as was demonstrated on experimental data [18], and based on data from simulation [16,17,19–23]. However, these methods rely on prior knowledge on the physical system, which is fundamentally problematic when trying to reveal new and unknown phase transitions and new phases of matter. This is manifested in the training process, which is based on known phase transitions. To address new phase transitions, where one cannot rely on previous knowledge acquired on other (known) systems, it was proposed to use unsupervised learning algorithms, i.e., learning from the data directly, without relying on any labeling. In machine learning, unsupervised learning was demonstrated to cluster data based on certain features of the systems [24,25]. Without prior knowledge, these approaches generally have limited success: on the one hand, unsupervised learning does not have a bias towards known phenomena, yet on the other hand, it does not produce high-quality distinction [26]. To overcome these challenges, it was suggested [27,28] to use a manifold-learning methodology called diffusion maps [29]. In a recent theory paper [28], diffusion maps was shown to retrieve the Thouless phase transition based on simulated measurements. However, it is still unclear whether this approach can handle true experimental data, where the noise is not well characterized and is often not homogeneous throughout the system, and most importantly—in many cases the edge states or parts of the spectrum are inaccessible to experiments.

Here, we use diffusion maps to identify the topological phase transition of a photonic system from true experimental data, without any prior assumptions on the system. We show that diffusion maps can identify the phase transition of a topological system, based on experimental excitations that do not include edge states. Likewise, we demonstrate identifiction based on random excitations or excitations limited to a small part of the spectrum. Finally, we test the performance of diffusion maps on known phase

transitions and conclude that indeed this technique can identify topological phase transitions from measurements, based on the data itself without any prior knowledge.

Diffusion maps is a kernel-based method for manifold learning. Generally, given a set of N snapshots of the evolution of a dynamical system $\{\boldsymbol{x}_i \in \mathbb{R}^D\}_{i=1}^N$, where i represents different sampling times of the observed data $\boldsymbol{x}$ and D is the dimension of each snapshot, diffusion maps seeks a low-dimensional representation of the observations, which should be isomorphic to the latent underlying intrinsic state of the system. In this work, we demonstrate that the low-dimensional representation obtained via diffusion maps facilitates the identification of topological phase transitions from experimental data, with high precision. Formally, given the set $\{\boldsymbol{x}_i\}_{i=1}^N$, we construct the kernel $\boldsymbol{K}[i,j] = \exp(-\|\boldsymbol{x}_i - \boldsymbol{x}_j\|^2/2\sigma^2)$ for all $i,j \in \{1,2,\ldots,N\}$, where $\|\cdot\|$ is a suitable norm operator. Here, σ is the Gaussian kernel scale that can be optimized for each model, but we set it consistently to be 5% of the median of all pairwise differences between the wave functions, i.e., $\sigma = 0.05$ median $(\{\|x_i - x_j\|\}_{i,j})$. A common practice is to use the Euclidean norm, but other norms can be used as well. We normalize $\boldsymbol{K}$ to be row stochastic according to $\boldsymbol{A}[i,j] = \boldsymbol{K}[i,j]/\sum_{s=1}^N \boldsymbol{K}[i,s]$, and apply eigendecomposition such that $\boldsymbol{A} = \boldsymbol{\Phi}\boldsymbol{\Lambda}\boldsymbol{\Phi}^{-1}$, where $\boldsymbol{\Lambda}$ is a diagonal matrix with nonincreasing eigenvalues $1 = \lambda_0 \geq \lambda_1 \geq \cdots \geq \lambda_{N-1}$. Finally, we define the mapping $\boldsymbol{x}_i \mapsto [\lambda_1^t \Phi[i,1], \cdots, \lambda_d^t \Phi[i,d]]$, where d is the desired dimensionality of the representation of the latent space, and t is a hyperparameter which controls the duration of the diffusion process [29]. Note that we ignore the first eigenvector $\boldsymbol{\phi}_0$ associated with λ_0, since it is a constant vector (due to the row normalization). In the latent space representation, the phase transitions can be detected, with good resolution, as sharp changes in the variation along the manifold.

We begin by demonstrating our method on simulated data described by the Haldane model, which is known to have a topological phase transition [2], and show how our approach can distinguish between the two phases, based only on partial data from the system.

The Haldane model is described by a honeycomb lattice with nearest neighbors (NN) and next-nearest neighbors (NNN) couplings that includes a nonzero phase [Fig. 1(a)]. This "Haldane phase" represents an applied (or synthetic) magnetic field which breaks time-reversal symmetry and opens a topological bandgap with edge states. On the other hand, if the honeycomb potential is staggered, that is, the honeycomb potential comprises of two triangular lattices of different on-site energies, the resultant potential breaks the inversion symmetry, which may close the topological gap and open a trivial one, thus causing a topological phase transition. The system is described by the Hamiltonian

$$H = t_1 \sum_{\langle n,m \rangle} a_n^\dagger a_m + t_2 \sum_{\langle\langle n,m \rangle\rangle} e^{-n\nu_{nm}\varphi} a_n^\dagger a_m + M \sum_n b_n a_n^\dagger a_n + \text{H.c.}, \tag{1}$$

where $a_n(a_n^\dagger)$ is the annihilation (creation) operator of site n, t_1 is the NN coupling and t_2 is the NNN coupling of the honeycomb lattice, M is the on-site staggered potential, b_n equal $+1(-1)$ for the $A(B)$ (triangular) sublattice, H.c. stands for Hermitian conjugate and φ is the Haldane phase. Here, the magnitude of φ is constant while its sign varies according to $\nu_{n,m} = \text{sign}(d_n \times d_m)_z$, where d_n and d_m are the vectors along the two bonds constituting the NNN couplings. In this model, detuning the parameter M corresponds to changing the ratio between inversion-symmetry

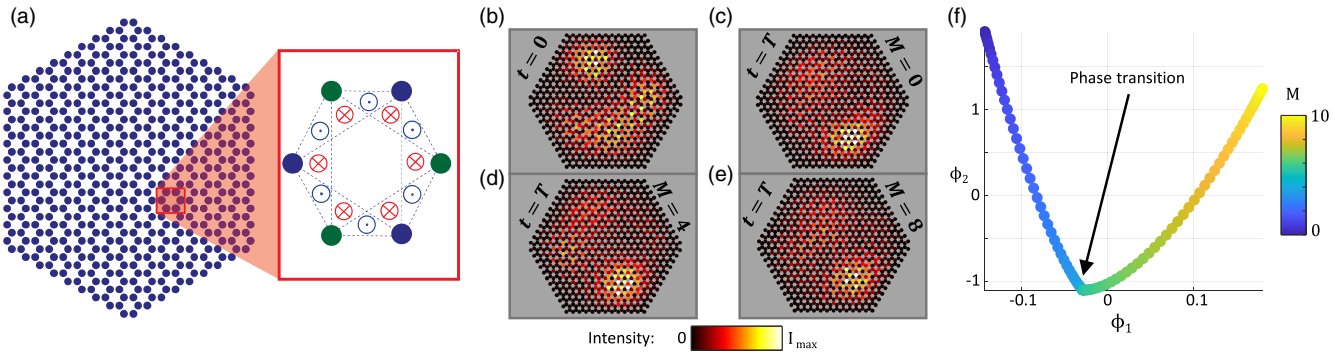

FIG. 1. (a) The Haldane unit cell: the green and blue lattice sites indicate the two underlying sublattices whose potential may be detuned from one another. The red and blue inward and outward arrows are direction of the nonuniform magnetic field. (b)–(e) Examples of the evolution of an arbitrary initial wave packet made of bulk states only. (b) Intensity distribution (in arbitrary units) of the initial bulk wave packet at $t = 0$. (c),(d) Intensity distribution at $t = T$ for the topological cases of $M = 0$ and $M = 4$. (e) Intensity distribution for the trivial case of $M = 8$, at $t = T$. The intensity distribution looks similar for all 4 cases of evolution in the bulk. (f) Scatter plot of the first two principal components of diffusion maps. The points are colored by the detuning in the honeycomb potential (magnitude of the detuning given by the color map). The cusp in (f), found by applying diffusion maps to the bulk propagation data [as (c)–(e)], is at the phase transition predicted by theory.

breaking and time-reversal breaking. Thus, for small M ($0 < M < M_{\text{critical}}$) time-reversal symmetry breaking is dominant and causes a topological band gap. However, when $M = M_{\text{critical}}$, the band gap closes completely, and above that value, the band gap opens again but this time as a trivial band gap [30].

To highlight the strength of our methodology, we demonstrate its ability to identify topological phase transitions based on data on bulk states only, without any data on edge states. To obtain data from the bulk only, we simulate the propagation of an initial wave packet ψ_0 in a finite lattice described by Eq. (1). The initial wave packet $\psi_i(0)$ is some random superposition of bulk states, so that it does not include any edge states (whose propagation has unique features when the phase is topological), making the detection of the topological phase of the system harder [Figs. 1(b)–1(e)]. Moreover, our initial wave packet is essentially noise, which means that it looks like noise also at the output—without any noticeable distinct features from which one could identify the topological state of the system. The simulated propagation is for a time period $T = 10$, for different values of M ranged uniformly between $M_1 = 0$ and $M_{100} = 10$, while φ is fixed at $\pi/2$. Changing the value of M_i can close the topological band gap and open a trivial band gap (and vice versa). We denote the discrete-time evolution of the initial wave packet $\psi_i(0)$ with $\boldsymbol{X}_i \in \mathbb{C}^{D\times N_T}$, where $D = 170$ is the number of sites, and $N_T = 1000$ is the number of time steps. Finally, we apply diffusion maps to the set $\{\boldsymbol{X}_i\}_{i=1}^{100}$, with $d = 2$. The number of dimensions d is chosen such that it is the minimal value that provides enough information for detection. Figure 1(f) shows the result displayed by a one-dimensional curve since effectively, there is only 1 degree of freedom, which is the value of M. The colors of the curve in Fig. 1(f) correspond to the different values, M_i. The most important feature in this figure is the cusp, which marks the presence of a topological phase transition. Diffusion maps identifies this phase transition from bulk data only, and the position of the cusp is at the theoretical phase transition of the system (for analysis of detection accuracy see Supplemental Material [31]). This result shows that the algorithm can detect the phase transition even without the most significant feature of the topological state—the edge states. Moreover, when the observed data set is relatively small, a similar result can be obtained with a variant of the analysis that relies on the spectral flow of the kernels of diffusion maps (see Supplemental Material [31]).

The result presented in Fig. 1 leads to the following question: how partial can the data be for the algorithm to detect the phase transition? To this end, we study the performance of the algorithm on data taken from a single eigenstate of the system, which represents the smallest possible part of the system's spectrum [Fig. 2(a)]. We repeat the same calculations as before, only this time the

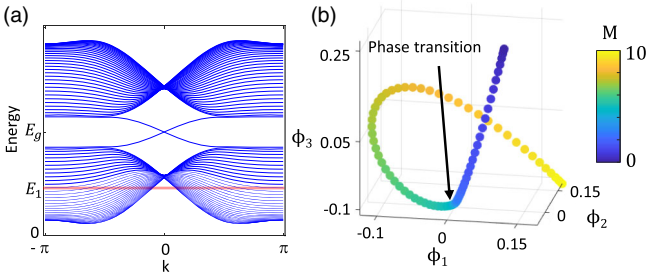

FIG. 2. (a) The spectrum of the Haldane model. The available data are associated with a small part of the spectrum around E_1, which is represented by the red shaded area. (b) Diffusion maps for the Haldane model, when observing the evolution of a single band eigenstate. The phase transition is at the sharp turn of the curve.

initial wave vector ψ_0 is an arbitrary single eigenstate of the Hamiltonian in Eq. (1). Figure 2(b) shows the obtained representation using diffusion maps. As before, we notice a cusp exactly at the theoretical phase transition. The appearance of a cusp at the phase transition facilitates automatic detection of the topological phase transition, which is offered by this methodology [Fig. 2(b)]. We observe a similar cusp also for phase transitions between larger Chern numbers and when varying other parameters such as the magnetic flux (see Supplemental Material [31]). Other methods that were studied numerically in the past can also offer a way to identify the phase transition, although using them on the Haldane model yields a gradual curve which (as we show later) does not pinpoint the phase transition (see Supplemental Material [31]). The other methods aim to provide a low-dimensional representation that preserves the pairwise distances between the high-dimnesional data. These approaches seem to lack the sensitivity required to detect the dynmical change in the high-dimensional data when the phase transition occurs. On the other hand, diffusion maps captures global relationships in the data, which enable it to identify the different dynamics before and after the phase transition. Up to this point, we have shown, on simulated data, that diffusion maps can identify topological phases even when the available data are extremely scarce, as is sometimes the case in experiments.

As mentioned earlier, one important application of machine learning methods is the need to study the phase transitions in true experimental systems without the ability to train a network (training set is unavailable) and without a known model (prescribing the relation between "input" and "output") to rely on. In addition, experimental data inevitably implies observation noise, which cannot be fully simulated—because experiments are never ideal, and many times noise is system specific at least in part. For these reasons, it is important to demonstrate diffusion maps on true experimental data and understand if it can work reliably or does it work only on ideal data that can only

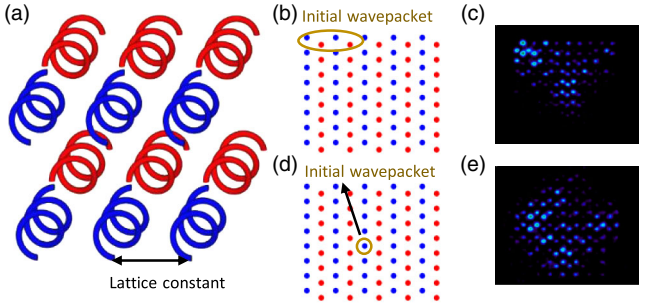

FIG. 3. (a) Helical waveguide array in a diagonal lattice with shifted helicity (as in Ref. [33]). (b),(d) location of input beam when the edge states are excited (b) and when the edge states are not excited (d). (c),(e) Example of experimental output intensity images, when the input wave packet is on the upper edge (c), and when the input is in the middle of the lattice (e).

be taken from simulations. To this end, we demonstrate that our approach successfully detects phase transitions in an experimental optical system that undergoes a topological phase transition [33]. We show that our methodology can detect the phase transition not only in cases where the data includes edge states (whose evolution is unique in topological systems, making the identification of the underlying topology much easier), but also when only bulk states are excited. The latter case is relevant for many experimental systems, in which the edge states cannot be directly excited and shows the robustness of our approach. The experimental results describing the phase transition were published in Ref. [33], and we use raw experimental data provided to us by the authors of Ref. [33]. The optical system is a lattice of evanescently coupled single-mode waveguides. By judiciously designing the three dimensional waveguide structure, it is possible to make the light evolve as electrons do in the anomalous Floquet topological insulator [33,34]. The waveguides are made helical in the evolution (propagation) axis z and are arranged in a diagonal square lattice [Fig. 3(a)]. In each unit cell, the helicity is shifted by $\pi/2$, giving rise to a topological phase transition in a line of a two dimensional parameter space, spanned by the wavelength and lattice constant.

The measurements are carried out in two types of initial excitations. The first type is focused mostly on the edge of the system—exciting the edge states directly and collecting the data on their evolution at the exit facet [Fig. 3(b)]. The second type of initial excitation is focused on exciting a single site in the middle of the lattice—not exciting any edge states at all [Fig. 3(d)]. For each type of initial excitation, the light intensity is imaged at the output facet [Figs. 3(c), 3(e)] for different lattice constants and wavelengths, forming a grid of measurements in parameter space [Figs. 4(a), 4(c)]. We emphasize that we use intensity data only, without interferometric measurements that would have revealed the phase of the output wave packets and could have made the algorithmic processing easier. We use

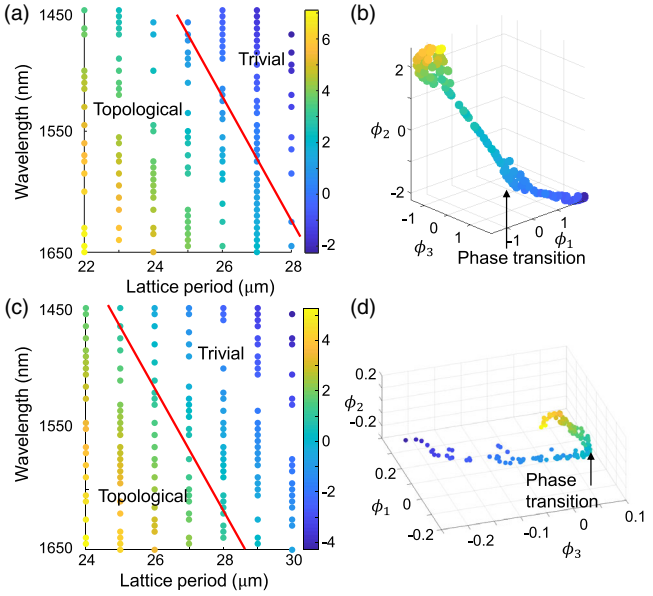

FIG. 4. (a) Data distribution in parameter space for the case of edge excitation [Figs. 3(b)–3(c)]; each point represents an experimental image. The color bar represents the distance in parameter space from the theoretical phase transition that is marked with a red line. (b) Diffusion maps applied to the experimental data. The color of the data points is the same as in (a). (c)–(d) Same as (a)–(b) only for the case where the bulk is excited [Figs. 3(d)–3(e)]. A second cusp (obtuse) is visible in (d) for distance values (color) of around 4. The obtuse cusp points to the destruction of the topoligcal phase due to enhanced NNN coupling.

diffusion maps on the recorded intensity images both for the measurements containing edge states [Fig. 4(b)] and for those without edge states, and observe the produced low dimensional manifold [Fig. 4(d)].

Technically, for each output image [e.g., Figs. 3(c), 3(e)], we extract a vector $\boldsymbol{x}_i \in \mathbb{R}^D$, where $D = 162$ is the number of sites, such that $\boldsymbol{x}_i[n]$ contains the intensity of the nth site. We apply diffusion maps to $\{\boldsymbol{x}_i\}_i$. Figure 4(b) displays the obtained diffusion maps representation with $d = 3$ when the excitation is on the edge. Similarly, the result for the excitation on the bulk is displayed in Fig. 4(d). As in the simulated results, in both cases, we notice a cusp point in the obtained representation. This cusp is located very close to the theoretical phase transition [Figs. 4(a), 4(c)]. Diffusion maps is robust enough to overcome the high level of irregularity in the experimental data, as demonstrated in Figs. 4(b), 4(d). Consequently, diffusion maps can detect a topological phase transition when the edge states are not excited, even from dilute data, and under true experimental conditions that inevitably contain disorder and experimental errors on the data. Figure 4(d) also displays an additional obtuse cusp, which is not as pronounced as the cusp indicating the topological phase transition associated with the Haldane model. This additional (obtuse) cusp is related to the destruction of the topoligcal phase due to enhanced NNN

coupling near the edge of the parameter range explored in the experimental system. Interestingly, diffusion maps was able to point to this unexpected behavior which is not covered by the physical model and is essentially a second topological transition, with an obtuse cusp.

To summarize, diffusion maps is a promising tool for detecting topological phase transitions, providing a powerful analysis tool for systems with limited access to the entire system and even without any data on the most distinct topological features—the edge states. We have shown that diffusion maps can overcome the errors that are inevitable in any experiment, and still identify the topological phase transition based on limited data. The experiment analyzed here was carried out in the context of photonics, but the approach is general and could work for any experimental system. Although we study a certain class of topological phase transitions, it is reasonable to conjecture that this approach can be extended to other types of phase transitions—both topological and non-topological. Finally, the big challenge is to employ diffusion maps to identify phase transitions in quantum many-body systems (such as many-body localization [35–37]), where theory can give only a limited indication of what to expect and what to examine in the experimental data. Indeed, the hope is that unsupervised machine learning will offer an avenue to discoveries based on analyzing experimental data from quantum many-body systems.

This work was supported by U.S. Air Force Office of Scientific Research (AFOSR), Israel Science Foundation (ISF), an Advanced Grant from the European Research Council (ERC), by the European Union's Horizon 2020 research grant agreement No. 802735 and by the Binational Science Foundation USA-Israel (BSF). O. Y. and E. L. are supported by the Adams Fellowship Program of the Israel Academy of Sciences and Humanities. We gratefully acknowledge the help of the authors of [33] for sharing their raw experimental data with us.

[*]These authors contributed equally to this work.

[1] D. J. Thouless, M. Kohmoto, M. P. Nightingale, and M. den Nijs, Phys. Rev. Lett. **49**, 405 (1982).
[2] F. D. M. Haldane, Phys. Rev. Lett. **61**, 2015 (1988).
[3] C. L. Kane and E. J. Mele, Phys. Rev. Lett. **95**, 146802 (2005).
[4] M. König, S. Wiedmann, C. Brüne, A. Roth, H. Buhmann, L. W. Molenkamp, X.-L. Qi, and S.-C. Zhang, Science **318**, 766 (2007).
[5] D. Hsieh, D. Qian, L. Wray, Y. Xia, Y. S. Hor, R. J. Cava, and M. Z. Hasan, Nature (London) **452**, 970 (2008).
[6] F. D. M. Haldane and S. Raghu, Phys. Rev. Lett. **100**, 013904 (2008).
[7] Z. Wang, Y. Chong, J. D. Joannopoulos, and M. Soljačić, Nature (London) **461**, 772 (2009).
[8] M. C. Rechtsman, J. M. Zeuner, Y. Plotnik, Y. Lumer, D. Podolsky, F. Dreisow, S. Nolte, M. Segev, and A. Szameit, Nature (London) **496**, 196 (2013).
[9] M. Hafezi, S. Mittal, J. Fan, A. Migdall, and J. M. Taylor, Nat. Photonics **7**, 1001 (2013).
[10] K. Lai, T. Ma, X. Bo, S. Anlage, and G. Shvets, Sci. Rep. **6**, 28453 (2016).
[11] G. Jotzu, M. Messer, R. Desbuquois, M. Lebrat, T. Uehlinger, D. Greif, and T. Esslinger, Nature (London) **515**, 237 (2014).
[12] M. Aidelsburger *et al.*, Phys. Rev. Lett. **111**, 185301 (2013).
[13] C. He, X. Ni, H. Ge, X.-C. Sun, Y.-B. Chen, M.-H. Lu, X.-P. Liu, and Y.-F. Chen, Nat. Phys. **12**, 1124 (2016).
[14] A. Kitaev, AIP Conf. Proc. **1134**, 22 (2009).
[15] Z. Gong, Y. Ashida, K. Kawabata, K. Takasan, S. Higashikawa, and M. Ueda, Phys. Rev. X **8**, 031079 (2018).
[16] J. Carrasquilla and R. G. Melko, Nat. Phys. **13**, 431 (2017).
[17] E. P. L. van Nieuwenburg, Y.-H. Liu, and S. D. Huber, Nat. Phys. **13**, 435 (2017).
[18] L. Li, Y. Yang, D. Zhang, Z.-G. Ye, S. Jesse, S. V. Kalinin, and R. K. Vasudevan, Sci. Adv. **4**, eaap8672 (2018).
[19] D.-L. Deng, X. Li, and S. Das Sarma, Phys. Rev. B **96**, 195145 (2017).
[20] Y. Zhang, R. G. Melko, and E.-A. Kim, Phys. Rev. B **96**, 245119 (2017).
[21] N. Yoshioka, Y. Akagi, and H. Katsura, Phys. Rev. B **97**, 205110 (2018).
[22] P. Zhang, H. Shen, and H. Zhai, Phys. Rev. Lett. **120**, 066401 (2018).
[23] D. Carvalho, N. A. Garcia-Martinez, J. L. Lado, and J. Fernández-Rossier, Phys. Rev. B **97**, 115453 (2018).
[24] L. Wang, Phys. Rev. B **94**, 195105 (2016).
[25] S. J. Wetzel, Phys. Rev. E **96**, 022140 (2017).
[26] M. J. S. Beach, A. Golubeva, and R. G. Melko, Phys. Rev. B **97**, 045207 (2018).
[27] O. Yair, E. Lustig, R. Talmon, and M. Segev, in *Conf. Lasers Electro-Optics* (Optical Society of America, San Jose, California, 2018), p. FM1E.6.
[28] J. F. Rodriguez-Nieva and M. S. Scheurer, Nat. Phys. **15**, 790 (2019).
[29] R. R. Coifman and S. Lafon, Appl. Comput. Harmon. Anal. **21**, 5 (2006).
[30] S. Stützer, Y. Plotnik, Y. Lumer, P. Titum, N. H. Lindner, M. Segev, M. C. Rechtsman, and A. Szameit, Nature (London) **560**, 461 (2018).
[31] See Supplemental Material at http://link.aps.org/supplemental/10.1103/PhysRevLett.125.127401 for more details about the performance of our approach and additional features of it which includes Refs. [32].
[32] D. Sticlet and F. Piéchon, Phys. Rev. B **87**, 115402 (2013).
[33] J. Noh, S. Huang, D. Leykam, Y. D. Chong, K. P. Chen, and M. C. Rechtsman, Nat. Phys. **13**, 611 (2017).
[34] L. J. Maczewsky, J. M. Zeuner, S. Nolte, and A. Szameit, Nat. Commun. **8**, 13756 (2017).

[35] Y. Bar Lev, G. Cohen, and D. R. Reichman, Phys. Rev. Lett. **114**, 100601 (2015).

[36] J. Choi, S. Hild, J. Zeiher, P. Schauß, A. Rubio-Abadal, T. Yefsah, V. Khemani, D. A. Huse, I. Bloch, and C. Gross, Science **352**, 1547 (2016).

[37] H. Bernien, S. Schwartz, A. Keesling, H. Levine, A. Omran, H. Pichler, S. Choi, A. S. Zibrov, M. Endres, M. Greiner, V. Vuletić, and M. D. Lukin, Nature (London) **551**, 579 (2017).